Stability Domain Calculations of Period-1 Ferroresonance in a Nonlinear Resonant Circuit

David A. N. Jacobson, *Member, IEEE*, Peter W. Lehn, *Member, IEEE*, and Robert W. Menzies, *Senior Member, IEEE*

***Abstract*—Catastrophic equipment failures continue to occur today due to ferroresonance even though this phenomenon has been extensively studied over the past 90 years. This paper is concerned with comparing analytical nonlinear dynamics methods with a two-dimensional (2-D) brute-force bifurcation diagram for displaying safety margins in a 2-D parameter space. A simplified single-phase model is used to represent the case of ferroresonance between a transformer and circuit breaker grading capacitor. Comparisons are made between the analytical method and EMTP simulations of an actual ferroresonant event.**

***Index Terms*—Approximation methods, capacitors, ferroresonance, nonlinear circuits, power system modeling, power system transients, power transformers.**

I. Introduction

BOUCHEROT [2] originally coined the word *ferroresonance* in 1920 to describe the phenomenon of two stable fundamental frequency operating points coexisting in a series resistor, nonlinear inductor, and capacitor circuit. The first published work, a 1907 paper by Bethenod [1], simply described the phenomenon as transformer resonance. Today, the term ferroresonance is firmly established in the power system engineer's vocabulary and is used to not only describe the jump to a higher current fundamental frequency state, but also bifurcations to subharmonic, quasi-periodic, and even chaotic oscillations in any circuit containing a nonlinear inductor.

The main objective of this paper is to attempt to answer the following question: "Given an operating point in a parameter space, what margin exists between the operating point and the nearest ferroresonant state?"

The catastrophic failure of a wound potential transformer at a 230-kV Manitoba Hydro substation [4] has made this more than an academic question—it is an important safety issue that must be addressed.

Time-domain simulation using detailed transformer and system models is the most accurate method for determining the probability of ferroresonance, aside from full-scale laboratory or system testing. Hundreds of simulations are required to get a sufficient feel for the effect of parameter variations. Each simulation, however, is no better than throwing a dart. The resulting scatter diagram does not give any information about behavior for cases which were not analyzed.

Manuscript received August 16, 1999.

D. A. N. Jacobson is with the System Planning Department, Manitoba Hydro, Winnipeg, MB R3C 2P4 Canada (e-mail: dajacobson@hydro.mb.ca).

P. W. Lehn is with the Department of Electrical and Computer Engineering, University of Toronto, Toronto, ON M5S 3G4 Canada (e-mail: lehn@ecf.toronto.edu).

R. W. Menzies is with the Department of Electrical and Computer Engineering, University of Manitoba, Winnipeg, MB R3T 5V6 Canada (e-mail: menzies@ee.umanitoba.ca).

Publisher Item Identifier S 0885-8977(02)05913-7.

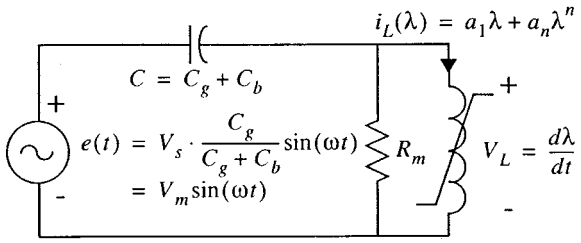

Fig. 1. Equivalent circuit model.

Direct calculation of the stability domains using Floquet theory or through calculation of the determinant of the Jacobian, as described by Van Craenenbroeck *et al.* [3], is a better technique. The only drawback is that the stability domains represent quasi-static bifurcations. Network switching, fault clearing, etc. may cause bifurcations to occur at different parameters than predicted by the quasi-static approach.

The paper will identify the differences between the time-domain and analytical quasi-static methods of calculating the fundamental frequency (i.e., period-1) ferroresonance stability domain boundary. A new analytical method is introduced which is based on modifying the slowly varying amplitude (SVA) method to include the effects of system dynamics.

II. Equivalent Circuit Model

The essential features of a transformer (PT)/grading capacitor model are shown in Fig. 1. A nonlinear inductor and a parallel resistor represent the PT. Total iron-core losses neglecting hysteresis effects are modeled by the linear resistor (R_m). An ideal source equivalent represents the system voltage (V_s), stray capacitance (C_b), and circuit breaker grading capacitance (C_g).

Given the simple circuit shown in Fig. 1, a nonlinear differential equation for flux linkage can be derived

$$\ddot{\lambda} + k\dot{\lambda} + C_1\lambda + C_3\lambda^n = G\cos(\omega t) \tag{1}$$

where $k = 1/R_mC$, $C_1 = \omega_b I_b a_1/CV_b$, $C_3 = \omega_b I_b a_n/CV_b$, and $G = \omega_b\omega V_m/V_b$.

III. Harmonic Balance Method

Hayashi [5] and Germond [6] have used the harmonic balance method to analytically determine approximate periodic solutions to the nonlinear differential equation given by (1). This method requires *a priori* knowledge of the harmonic content of the final state and does not consider the possibility of ferroresonance being switching surge induced.

TABLE I
SYSTEM PARAMETERS

iron-core loss resistance	R_m	*11.9E6 Ω*
grading capacitance	C_g	*2000 pF*
stray capacitance	C_b	*10450 pF*
base voltage	V_b	*187794.2 V*
base current	i_b	*1.0 A*
source voltage	V_s	*173521.8 V*
system, base frequency	ω,ω_b	*376.991 rad/sec*
saturation curve parameter	a_1	*0.1*
saturation curve parameter	a_3	*1.0*
saturation curve parameter	n	*3*

A first-order solution for (1) can be assumed to be of the form

$$\lambda(t) = a\cos(\omega t) + b\sin(\omega t) = r\cos(\omega t + \phi). \quad (2)$$

The basic procedure of harmonic balance is to substitute (2) into (1) and equate terms of $\cos(\omega t)$ and $\sin(\omega t)$. Since this is a first-order approximation, third harmonics are ignored. After equating terms and substituting r^2 for $a^2 + b^2$, the following equation results:

$$\left(\left(\omega^2 - C_1\right)^2 + k^2\omega^2\right) r^2 - 2C_3 d_1 \left(\omega^2 - C_1\right) r^{n+1} + C_3^2 d_1^2 r^{2n} = G^2. \quad (3)$$

The binomial expansion is used to derive d_1 [12]

$$d_1 = \left(\frac{1}{2}\right)^{n-1} \binom{n}{\frac{n-1}{2}}. \quad (4)$$

Real values of r that satisfy (3) correspond to equilibrium points or solutions to the original differential equation.

A particular example will illustrate the procedure. The parameters listed in Table I were substituted into (3). A third-order polynomial approximation of the saturation curve results in (1) being of the same form as Duffing's equation [9].

Three solutions were found for $r : \{-0.172, -0.924, 1.095\}$. Floquet theory [5], [9] can be used to calculate the stability of the solutions to the first variational equation [i.e., linearized form of (1)].

IV. SLOWLY VARYING AMPLITUDE (SVA) METHOD

The SVA method is an averaging method that is useful for visualizing the nature of solutions near equilibrium points for weakly nonlinear problems. The method was originally conceived by Krylov and Bogoliubov in 1937 and was extended by Bogoliubov and Mitropolsky in 1955 and is also referred to as the *KBM method* [9], [10].

The method begins by assuming that a solution to the differential equation, given by (1), can be written in the form

$$\lambda(t) = a(t)\cos(\omega t) + b(t)\sin(\omega t) \quad (5)$$

where $a(t)$ and $b(t)$ have SVAs compared with $\cos(\omega t)$ and $\sin(\omega t)$.

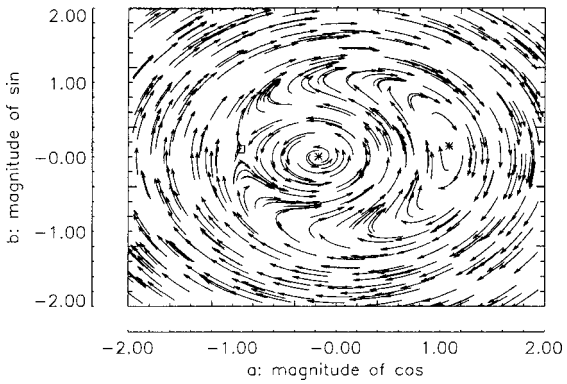

Fig. 2. Paths in the van der Pol plane (Cg: 2000 pF and V_s: .924 p.u.).

The method proceeds as in the harmonic balance method. The solution is substituted into the differential equation and coefficients of $\sin(\omega t)$ and $\cos(\omega t)$ are equated. Second-order derivatives of a and b, terms in $\cos(3\omega t)$ and $\sin(3\omega t)$ and terms kda/dt and kdb/dt are neglected.

After equating terms and solving for the first derivative of a and b, the following averaged equations result:

$$\dot{a} = \frac{-b}{2\omega}\left(\left(\omega^2 - C_1\right) - C_3\left(a^2 + b^2\right)^{(n-1)/2} d_1\right) - \frac{ka}{2} \quad (6)$$

$$\dot{b} = \frac{a}{2\omega}\left(\left(\omega^2 - C_1\right) - C_3\left(a^2 + b^2\right)^{(n-1)/2} d_1\right) - \frac{kb}{2} + \frac{G}{2\omega}. \quad (7)$$

A typical portrait in the a-b phase plane is shown in Fig. 2. The plane is also known as the van der Pol plane, named after Balthasar van der Pol (1889–1959), a Dutch physicist who studied the dynamics of electronic oscillators in the 1920s.

The fixed points calculated previously using the harmonic balance method are also displayed. The stability of each is immediately apparent by examining the behavior of the velocity field in a small neighborhood around the fixed points. The coordinates of the fixed points are calculated by substituting $r^2 = a^2 + b^2$ into (6) and (7) and solving for a and b where the first derivatives are zero.

The SVA method has transformed a nonautonomous differential equation into an autonomous differential equation. Fixed points replace limit cycles. The stability of the fixed points can be determined by performing a Taylor expansion in a small neighborhood around the fixed points. The fixed points are stable if the eigenvalues of the Jacobian lie in the left half of the complex plane.

Table II summarizes the calculations made to determine the stability of the fixed points in the van der Pol plane.

The calculations confirm the conclusions drawn from observing the behavior in the van der Pol plane.

V. BIFURCATION THEORY

A *bifurcation* is the abrupt change in the qualitative nature of the system's final operating state as a system parameter is quasi-statically varied. A *bifurcation diagram* records the locations of all bifurcations over a range of parameter values.

TABLE II
FIXED POINT CLASSIFICATION

fixed points		eigenvalues	classification
a	*b*		
1.0857	0.1447	-3.37 ±j101.9	stable spiral
-0.1723	0.0036	-3.37 ±j157.5	stable spiral
-0.9185	0.1031	82.29, -89.04	unstable saddle point

Two main techniques exist for the calculation of a bifurcation diagram. One is based on the principle of continuation [3], and the other is based on experimentation or time-domain simulation. Bifurcation diagrams generated using commercial time-domain simulation packages, such as EMTDC [7] or EMTP [4], are sometimes referred to as *brute-force bifurcation diagrams*. Samples of the system state variables are taken once per 60-Hz cycle as a parameter is slowly varied. This is sometimes referred to as *Poincaré sampling*.

A bifurcation diagram can also be found analytically by solving (3) as a bifurcation parameter (e.g., source voltage) is varied. Fig. 3 illustrates a typical bifurcation diagram.

As the bifurcation parameter is slowly increased from zero, a jump in flux linkage occurs at the first turning point. Similarly, as the bifurcation parameter is slowly decreased from a high value, a jump decrease in flux linkage occurs at the second turning point. The result is a hysteretic-type pattern.

The type of bifurcation just illustrated is referred to as a *jump resonance* [8] or a *cyclic fold* or *saddle-node* bifurcation [9]. At the turning point, one eigenvalue of the linearized circuit is attempting movement into the right half of the complex plane.

The turning points shown in Fig. 3 can be calculated as a function of two parameters (e.g., grading capacitance and source voltage). Since an equation that relates source voltage to flux linkage exists [see (3)], the critical points can be calculated by differentiating with respect to flux linkage. Critical points can also be calculated by solving three nonlinear algebraic equations (i.e., (6) and (7) and the determinant of the Jacobian are equated to zero).

A projection of the first turning point on the grading capacitance-source voltage parameter plane is shown in Fig. 4. The curve is known as a *bifurcation line* or a *stability domain boundary* and it indicates the parameter values required to spontaneously jump to period-1 ferroresonance.

In order to illustrate the effect of de-energizing a PT on the period-1 stability domain boundary, a brute-force bifurcation diagram [4] is constructed and is displayed in Fig. 5. Individual 1.5-s time-domain simulations are computed for discrete changes in C_g and V_s. A symbol is used to represent the periodicity of the final state. The example in Fig. 5 is the result of 7260 individual time-domain simulations.

Prior to the circuit breaker opening, the grading capacitor is short-circuited. Following circuit breaker opening, the circuit configuration is equivalent to Fig. 1.

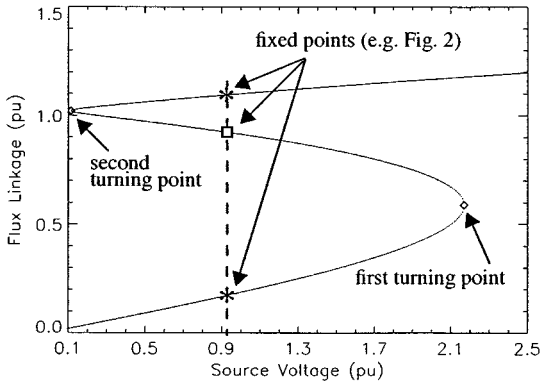

Fig. 3. Classic bifurcation diagram (C_g: 2000 pF).

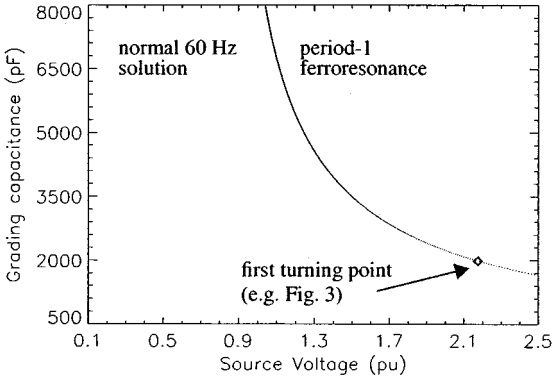

Fig. 4. Quasi-static stability domain boundary.

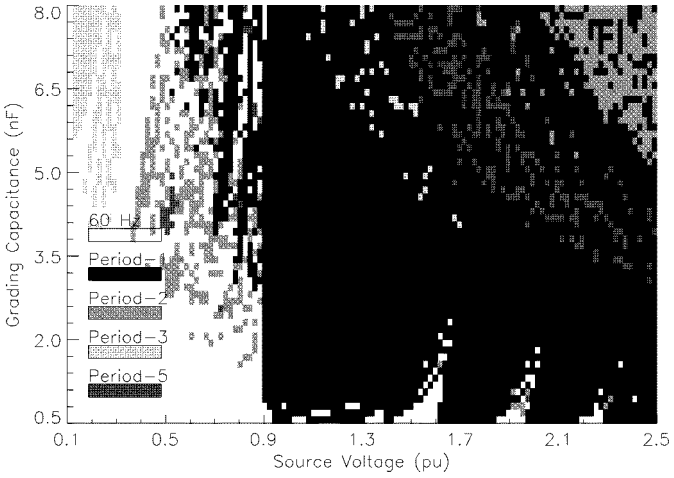

Fig. 5. Brute-force 2-D bifurcation diagram.

The quasi-static stability domain boundary shown in Fig. 4, determined by classical bifurcation theory, is seen to yield only a very crude approximation to the actual transition from no ferroresonance to period-1 ferroresonance. The large discrepancy between the simulation results and those predicted by classical bifurcation theory stem from the theory's underlying quasi-static assumption and its inability to account for transient phenomena, such as the opening of a circuit breaker.

VI. Separatrix Calculation

Given a particular set of system parameters, a pair of initial conditions can be chosen on the two-dimensional (2-D) phase plane and the trajectory leading to a new steady-state can be calculated. The *basin of attraction* is the set of initial conditions leading to a particular final operating state or attractor.

The van der Pol diagram shown in Fig. 2 is meant to graphically indicate the stability of fixed points; however, it can also be used to illustrate the concept of a basin of attraction. For the set of parameters chosen, there are two stable spiral attractors indicated by asterisks. Two regions or basins of initial conditions exist in Fig. 2 such that the trajectories will converge onto a specific attractor. The curve separating the two basins is called the *separatrix*.

The separatrix may be sketched from the velocity field, or it may be computed by time-domain simulation of (6) and (7) for decreasing time. If the simulation approach is used, the system states must be initialized to correspond to the unstable fixed point plus a small deviation along the stable eigenvector associated with this point.

The basin of attraction can be used to improve upon the prediction of ferroresonance as simply a jump phenomena, since it accounts for the transients that occur. These transients typically result in a premature transition into period-1 ferroresonance and should not be neglected.

Depending on the particular ferroresonant circuit, the initial conditions may not realistically cover the entire phase plane. For example, for the case where a transformer is being de-energized, the initial conditions are prescribed at the instant the circuit breaker opens. Therefore, only two initial conditions are possible in a single-phase model assuming the breaker opens exactly at a current zero.

Assuming the stray capacitance dominates the impedance of the three parallel elements, the flux linkage will be zero and the rate-of-change of flux linkage will be maximum and equal to the source voltage (V_s) at the instant the circuit breaker opens. The instantaneous initial conditions, however, are not mapped onto the van der Pol plane.

A Poincaré sampled $d\lambda/dt$ versus λ plane can be thought of as a subset of the van der Pol plane. An example is given in Fig. 6. The sampled points can be laid on top of the van der Pol diagram given in Fig. 2 and the true trajectory sketched using the velocity field lines. The straight line segments shown in Fig. 6 only indicate the direction of movement of the trajectory.

By selecting sampling to occur at $\omega t = 0$, the $d\lambda/dt$ term in the initial state is zero. For the case of a transformer being de-energized, the initial flux linkage in the nonlinear inductor is equal to the integral of the source voltage (i.e., $-V_s/\omega$ or $-V_s/V_b$ p.u.). Referring to Fig. 7, this initial condition lies on the a-axis near the separatrix.

An increase in source voltage magnitude will cause a leftward shift of the initial condition, resulting in a crossing of the separatrix into the period-1 basin of attraction. Low values of source voltage will result in the nonferroresonant state.

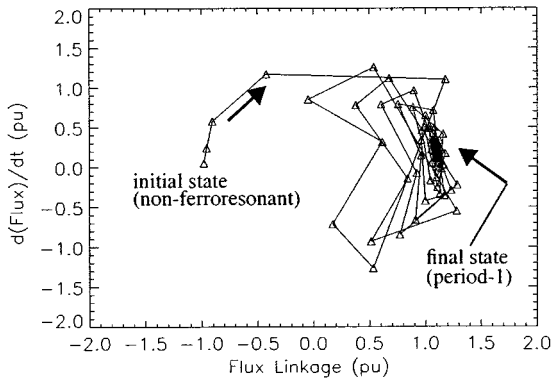

Fig. 6. Poincaré sampled trajectory (C_g: 2000 pF and V_s: .90 p.u.).

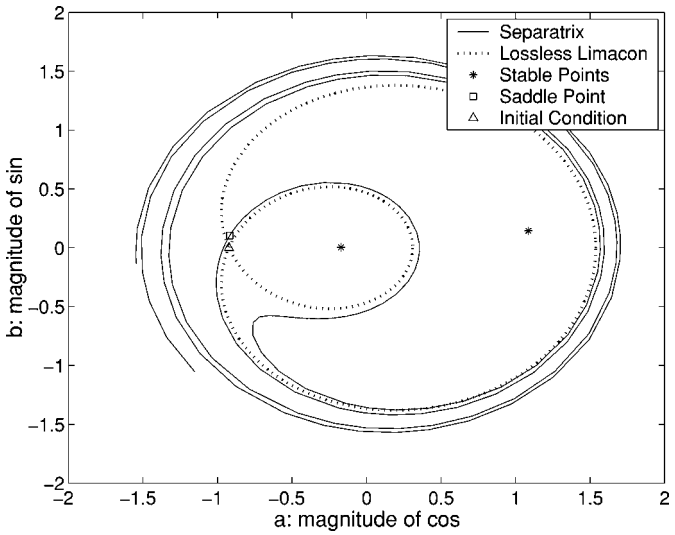

Fig. 7. Separatrices (C_g: 2000 pF and V_s: .924 pu).

The separatrix is also affected by variations in the source voltage. Consequently, an iterative approach would be required to determine at what voltage level the initial conditions leave the basin of attraction of the nonferroresonant state. Each iteration would require simulation of the system equations.To circumvent this complexity, a closed-form solution is sought for describing the separatrix as some function of the system parameters. The analysis is simplified by assuming the system to be conservative [i.e., $k = 0$ in (6) and (7)].

The separatrix has thus far been determined by reverse-time integration from the saddle point. In the conservative case, however, its general shape likens that of the geometrical figure known as the *Limacon of Pascal*. This likeness identifies the following class of functions as candidates for the solution of the separatrix:

$$a(\theta) = \alpha \cdot \cos\theta + \beta \cdot \cos 2\theta \tag{8}$$

$$b(\theta) = \alpha \cdot \sin\theta + \beta \cdot \sin 2\theta. \tag{9}$$

These general functions are then substituted into the lossless reverse-time differential equations, derived from (6) and (7), for the case when n is three.

Solving for the constants α and β yields the following two equations:

$$\beta = \sqrt[3]{\frac{-2G}{3C_3} + \sqrt{\left(\frac{4(C_1-\omega^2)}{9C_3}\right)^3 + \left(\frac{2G}{3C_3}\right)^2}} + \sqrt[3]{\frac{-2G}{3C_3} - \sqrt{\left(\frac{4(C_1-\omega^2)}{9C_3}\right)^3 + \left(\frac{2G}{3C_3}\right)^2}} \quad (10)$$

$$\alpha = \sqrt{\frac{8G}{3C_3\beta}}. \quad (11)$$

With the above values of α and β, (8) and (9) are used to plot the exact separatrix for the conservative system in Fig. 7. Fig. 7 also compares the estimated separatrix from theory with the separatrix for the dissipative system. It may be seen that the lossless separatrix yields a slightly conservative estimate for the basin of attraction of the nonferroresonant operating point.

The initial conditions lie on the boundary between nonferroresonance and period-1 ferroresonance when

$$\frac{-V_s}{V_b} = \alpha \cdot \cos\theta_1 + \beta \cdot \cos 2\theta_1 \quad (12)$$

where α and β are functions of G, which is in turn a function of the system voltage and grading capacitance. The critical angle (θ_1) lies between zero and π and is calculated by finding the zero of (9).

Equation (12) implicitly defines the critical system voltage at which period-1 ferroresonance first occurs, as a function of the system parameters. Solving for this critical system voltage as a function of the grading capacitance yields a modified stability domain boundary, as depicted in Fig. 8.

Using the lossless separatrix calculation method, the calculated stability domain boundary is found to be grading capacitance invariant within the range 500 pF–8000 pF. This feature is also strongly evident in the brute-force diagram given in Fig. 5. For grading capacitance less than 2500 pF, the error between the brute-force boundary and the calculated boundary is not significant.

As the grading capacitance increases, a period-2 ferroresonance mode develops. The presence of subharmonics tends to shift the fundamental frequency boundary to the left.

When subharmonic attractors are considered, the basin boundaries become extremely complex as demonstrated by Hayashi [5]. It is demonstrated in [12] that the presence of subharmonics causes oscillations in the separatrix. The oscillations lead to multiple crossings of the separatrix on the negative flux linkage axis near the saddle point.

For low values of grading capacitance, the brute-force stability domain boundary also shows the possibility of nonferroresonant modes existing at higher source voltages. By examining Fig. 7, this behavior can be predicted from the reverse-time integration of the dissipative system equations. The basin of attraction for the two fundamental frequency oscillation modes spiral out in the a-b phase plane. If the initial source voltage is high enough, there is a finite probability that the initial conditions will lie in either the nonferroresonant or period-1 ferroresonant basin.

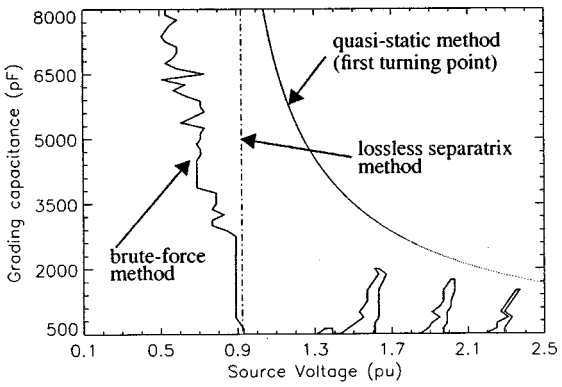

Fig. 8. Stability domain boundary comparison ($n = 3$).

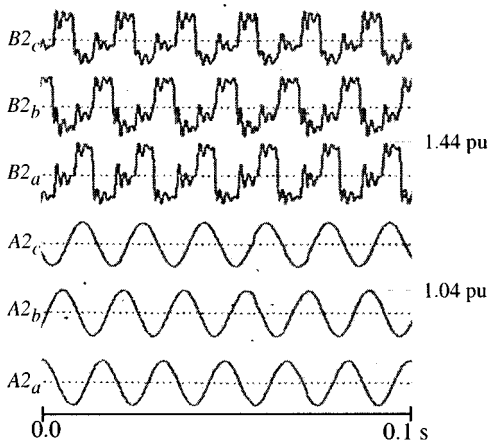

Fig. 9. Field recordings of bus voltages.

VII. Practical Example

The analytical method described in the previous sections will be applied to a practical example of ferroresonance.

On August 5, 1995, at 14:18, a 4.16-kV breaker failed to latch while attempting to energize a 1500-kW induction motor at the Dorsey Converter Station in Manitoba, Canada [11]. As a result, 11 230-kV breakers opened to clear bus B2 to which the 230-kV/4.16-kV transformer (SST1) was connected.

Noise levels coming from SST1 were noticeably higher than normal and higher than the nearby loaded SST2 immediately following the 230-kV bus de-energization. Recordings given in Fig. 9 show high distortion and overvoltages near 1.5 p.u. indicating a steady-state mode of ferroresonance had developed.

An EMTP model was developed and successfully modified to match field recordings of the disturbance [11]. A single-line diagram of the EMTP model is given in Fig. 10.

The approach taken in modeling the transformer's magnetization curve is to find a polynomial that closely follows the manufacturers data and best represents recordings from an inrush or ferroresonance test. A thirteenth-order two-term polynomial is found to be a reasonable representation. The parameters used are: $a_1 = .002$, $a_{13} = .0024$, $n = 13$, and $i_b = 35.5$ A.

Iron-core losses of the station service transformers are 17 kW at nominal voltage. A more detailed model of iron-core losses is required to match the recorded transients. At the same instant that the oscillation mode changes to ferroresonance, additional

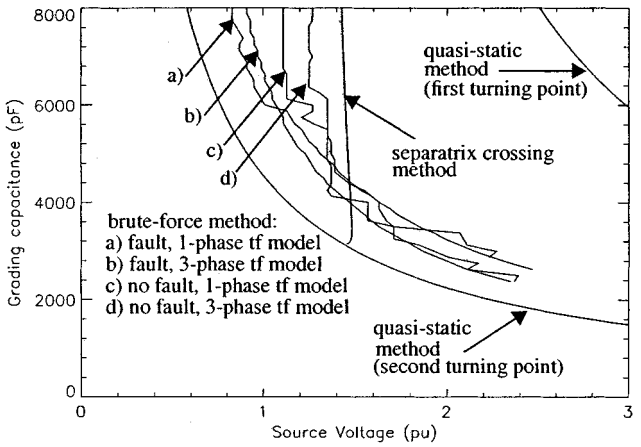

Fig. 10. Comparison of stability domain boundary locations ($n = 13$).

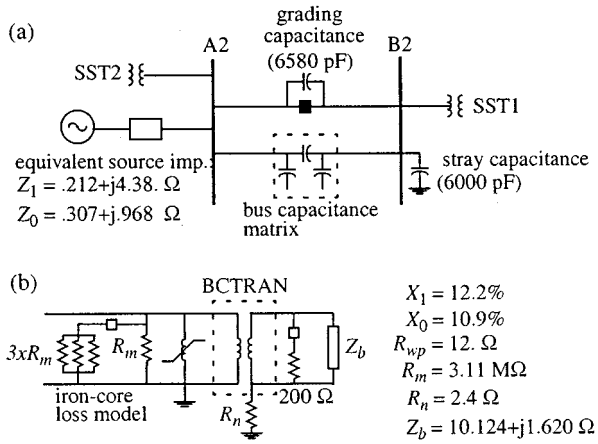

Fig. 11. Single-line diagram of the August 5, 1995, Dorsey disturbance showing (a) main circuit components and (b) model of station service transformer.

resistance is switched on in parallel with the existing linear iron-core loss resistor. A more detailed discussion of iron-core loss modeling can be found in [11] and [12].

When bus B2 is de-energized, it remains capacitively coupled to the 443-m parallel A2 bus. A bus capacitance matrix is used to model the capacitive coupling [4]. The equivalent phase-to-ground capacitance (C_{pg}) is 5316 pF and the mutual capacitance (C_m) is 1108 pF. The equivalent positive sequence capacitance-to-ground is $C_{pg} + C_m$ or 6424 pF. Therefore, the effective stray capacitance (C_b) used in (1) is 12 424 pF.

The period-1 stability domain boundary is calculated using several methods with the results displayed in Fig. 11.

For the brute-force method, the detailed 3-phase EMTP model is used. Both faulted and unfaulted clearing of the SST are compared, in order to determine the sensitivity to initial conditions.

In addition, comparison is made between a 3-phase BCTRAN transformer model and a model using three single-phase transformers. The location of the stability domain boundary does not depend greatly on the type of model chosen.

Three analytically calculated stability domain boundaries are shown in Fig. 11.

A more general technique is used to calculate the Limacon and determine the parameter values that result in a crossing of the separatrix [11]. The Limacon of Pascal is an exact solution for the third-order conservative case and is a good approximation for the nonconservative case even when higher orders of n are considered. The curve shown estimates the stability domain boundary for the case of de-energizing an unfaulted transformer.

Other separatrix crossing points can also easily be calculated. However, the majority of transformer de-energizations are due to unfaulted clearing. Our focus has been to identify this transition point and in spite of several assumptions and simplifications, the proposed analytical method does provide a much better estimate than projection of the first turning point.

The projection of the second turning point is a good approximation to the faulted brute-force stability domain boundary. The analytical calculation ignores winding losses in the transformer which leads to a conservative estimate.

Fig. 11 shows the sensitivity to the main variable parameters (i.e., C_g and V_s). Sensitivity to variation in stray capacitance is not significant [11].

The sensitivity to initial conditions is indicated by the spread between the faulted and unfaulted brute-force stability domain boundaries. The sensitivity increases with increasing C_g.

The most significant unknown is the value of iron-core losses during ferroresonance. In the example presented, field measurements were available and were used to adjust the iron-core loss model until the measurements could be duplicated. Depending on the transformer and the mode of ferroresonance, a four-fold increase in iron-core losses may be inappropriate. Further research into iron-core loss modeling is recommended.

One application of the method has been to divide the parameter plane into several regions depending on the probability of developing ferroresonance. Using this technique, a decision was made to switch 200 Ω resistors rather than have them permanently connected [11].

VIII. Conclusions

Quasi-static analytical approaches can be used to give a quick indication of the locations of domains of different ferroresonant states as a function of a set of parameters. However, these approaches do not give an accurate indication of safety margins if large-signal perturbations are considered. A brute-force 2-D bifurcation diagram is an ideal tool for displaying margins between ferroresonant and nonferroresonant states. However, an extensive number of long duration simulations are required in the calculation of such a diagram.

The difference in the period-1 stability domain boundary calculated by the quasi-static and brute-force technique is attributed to the initial conditions at the time of the perturbation. Different final operating states are possible depending on the basin of attraction in which the initial conditions lie.

The Limacon of Pascal is a good approximation to the geometric shape of the basin of attraction of the period-1 ferroresonant attractor and can be used to analytically calculate a better approximation of the stability domain boundary.

A general set of averaged equations is given that permit the analysis of an nth order two-term polynomial approximation of the saturation curve.

The analytical method has been compared successfully against a practical example of ferroresonance. The simple system representation and first-order approximations are sufficiently accurate to predict the behavior of a complete 3-phase detailed system model.

Future work is recommended to focus on measuring the effective iron-core losses during different ferroresonance modes for different types of transformers with the goal of creating an improved iron-core loss model.

REFERENCES

[1] J. Bethenod, "Sur le transformateur à résonance," *L'Éclairage Électrique*, vol. 53, pp. 289–96, Nov. 1907.

[2] P. Boucherot, "Existence de deux régimes en ferrorésonance," *Rev. Gen. de L'Élec.*, vol. 8, no. 24, pp. 827–828, Dec. 1920.

[3] T. Van Craenenbroeck, W. Michiels, D. Van Dommelen, and K. Lust, "Bifurcation analysis of 3-phase ferroresonant oscillations in ungrounded power systems," *IEEE Trans. Power Delivery*, vol. 14, pp. 531–536, Apr. 1999.

[4] D. A. N. Jacobson, D. Swatek, and R. Mazur, "Mitigating potential transformer ferroresonance in a 230 kV converter station," in *Computer Analysis of Electric Power System Transients: Selected Readings*. Piscataway, N.J: IEEE Press, 1997, pp. 359–365.

[5] C. Hayashi, *Nonlinear Oscillations in Physical Systems*. New York: McGraw-Hill, 1964.

[6] A. Germond, "Computation of ferroresonant overvoltages in actual power systems by Galerkin's method," in *Proc. IEEE PICA Conf.*, New Orleans, LA, June 1975, pp. 127–135.

[7] P. S. Bodger, G. D. Irwin, D. A. Woodford, and A. M. Gole, "Bifurcation route to chaos for a ferroresonant circuit using an electromagnetic transients program," *Proc. Inst. Elect. Eng.—Proc. Generation, Transmission, and Distribution*, vol. 143, pp. 238–242, May 1996.

[8] G. Swift, "An analytical approach to ferroresonance," *IEEE Trans. Power App. Syst.*, vol. 88, pp. 42–46, Jan. 1969.

[9] J. Guckenheimer and P. Holmes, *Nonlinear Oscillations, Dynamical Systems and Bifurcations of Vector Fields*, 3rd ed. New York: Springer-Verlag, 1990.

[10] N. Minorsky, *Nonlinear Oscillations*. New York: Van Nostrand, 1962.

[11] D. A. N. Jacobson and R. W. Menzies, "Investigation of station service transformer ferroresonance in Manitoba Hydro's 230-kV Dorsey Converter Station," in Proc. Int. Conf. Power Systems Transients, Rio de Janeiro, Brazil, June 24–28, 2001.

[12] D. A. N. Jacobson, "Field testing, modeling, and analysis of ferroresonance in a high-voltage power system," Ph.D. dissertation, University of Manitoba, Winnipeg, MB, Canada, 2000.

David A. N. Jacobson (S'84–M'90) received the B.Sc. degree in electrical engineering (with distinction) and the M.Sc. and Ph.D. degrees from the University of Manitoba, Winnipeg, MB, Canada, in 1988, 1990, and 2000, respectively.

He joined Manitoba Hydro, Winnipeg, in 1990, where he is currently a Grid Supply Enhancement Engineer. He was a Visiting Researcher with the Siemens Power System Planning group in Erlangen, Germany, in 1994. His research interests include nonlinear dynamics, power system control, and FACTS devices.

Dr. Jacobson has been a registered Professional Engineer in the province of Manitoba since 1992.

Peter W. Lehn (M'88) received the B.Sc. and M.Sc. degrees in electrical engineering from the University of Manitoba, Winnipeg, MB, Canada, in 1990 and 1992, respectively, and the Ph.D. degree from the University of Toronto, Toronto, ON, Canada, in 1999.

From 1992 to 1994, he was with the Network Planning Group of Siemens AG, in Erlangen, Germany. Presently, he is an Assistant Professor at the University of Toronto. His research interests include analytical modeling of nonlinear and switched circuits.

Robert W. Menzies (M'67–SM'75) received the B.Eng. degree in electrical engineering from McMaster University, Hamilton, ON, Canada, in 1964, and the Ph.D. degree from the University of St. Andrews, St. Andrews, U.K., in 1967.

Since 1967, he has been with the University of Manitoba, Winnipeg, MB, Canada, where he is presently Professor and Head of Electrical and Computer Engineering. He has worked with Westinghouse Canada on induction motor optimization, with Brown Boveri on inverter drives for locomotives and static compensators, and with ABB Drives on large GTO inverter drives.

Dr. Menzies is a registered Professional Engineer in the province of Manitoba.